

Simulation to the Cyclic Deformation of Polycrystalline Aluminum Alloy Using Crystal Plasticity Finite Element Method

Juan Luo, Guozheng Kang*, Mingxing Shi

School of Mechanics and Engineering, Southwest Jiaotong University, Chengdu 610031, China

*Corresponding author: Kang GZ, E-mail address: guozhengkang@home.swjtu.edu.cn;

Tel: 86-28-87603794; Fax: 86-28-87600797

Abstract

A crystal plasticity based finite element model (i.e., FE model) is used in this paper to simulate the cyclic deformation of polycrystalline aluminum alloy plates. The Armstrong-Frederick nonlinear kinematic hardening rule is employed in the single crystal constitutive model to capture the Bauschinger effect and ratcheting of aluminum single crystal presented under the cyclic loading conditions. A simple model of latent hardening is used to consider the interaction of dislocations between different slipping systems. The proposed single crystal constitutive model is implemented numerically into a finite element code, i.e., ABAQUS. Then, the proposed model is verified by comparing the simulated results of cyclic deformation with the corresponding experimental ones of a face-centered cubic polycrystalline metal, i.e., rolled 5083 aluminum alloy. In the meantime, it is shown that the model is capable of predicting local heterogeneous deformation in single crystal scale, which plays an important role in the macroscopic deformation of polycrystalline aggregates. Under the cyclic loading conditions, the effect of applied strain amplitude on the responded stress amplitude and the dependence of ratcheting strain on the applied stress level are reproduced reasonably.

Keywords: Crystal plasticity; Cyclic deformation; Finite element; Face-centered cubic metal

Introduction

It is significant to study the cyclic deformation of metals for their extensive uses as engineering components subjected to cyclic loadings. In the last decades, many researches have been accomplished to observe the cyclic deformation of metals both experimentally and theoretically. However, many existing constitutive models are phenomenological versions, such as Chaboche and Dang Van (1979), Chaboche and Nouailhas (1989), and Abdel-Karim and Ohno (2000). These models do not give direct insight into the physical mechanism of cyclic plastic deformation. Recently, Cailletaud and Sai (2008) and Kang et al. (2010) proposed crystal plasticity based constitutive models to investigate the ratcheting of polycrystalline alloys by adopting explicit scale transition rules. However, the employed explicit scale transition rules are formulated with some simple assumptions, which cannot capture the real physical nature of elastic and plastic accommodations occurred between single crystal grains. To consider such accommodations reasonably, a crystal plasticity finite element method is a good candidate.

Therefore, in this work, based on the previous work done by Armstrong and Frederick (1966), Peirce et al. (1983) and Huang (1991), a micro-mechanically based cyclic single crystal viscoplastic constitutive model is implemented numerically into the finite element (FE) code ABAQUS, to predict the responses of polycrystalline metals under cyclic strain-controlled and stress-controlled loading. The model is verified by comparing the FE simulations with corresponding experimental results of face-centered cubic (FCC) polycrystalline aggregates, i.e., rolled 5083 aluminum alloy plate, carried out in the previous work by Lu et al. (2013).

Single crystal constitutive model

In the framework of small perturbation, the total strain $\boldsymbol{\varepsilon}$ is divided additively into an elastic part $\boldsymbol{\varepsilon}^e$ and visco-plastic part $\boldsymbol{\varepsilon}^{vp}$, i.e.,

$$\boldsymbol{\varepsilon} = \boldsymbol{\varepsilon}^e + \boldsymbol{\varepsilon}^{vp} \quad (1)$$

The relation between the elastic strain $\boldsymbol{\varepsilon}^e$ and the stress $\boldsymbol{\sigma}$ is given by the Hooke's law

$$\boldsymbol{\varepsilon}^e = \mathbf{C}^{-1} : \boldsymbol{\sigma} \quad (2)$$

where \mathbf{C} is the fourth-rank tensor of elastic moduli. Since the dislocation slip is the main source of plastic deformation for the aluminum alloy at low temperatures, the visco-plastic strain rate can be obtained via the following expression,

$$\dot{\boldsymbol{\varepsilon}}^{vp} = \sum_{\alpha=1}^N \mathbf{P}^{\alpha} \dot{\gamma}^{\alpha} \quad (3)$$

$$\mathbf{P}^{\alpha} = \frac{1}{2} (\mathbf{m}^{\alpha} \otimes \mathbf{n}^{\alpha} + \mathbf{n}^{\alpha} \otimes \mathbf{m}^{\alpha}) \quad (4)$$

where \mathbf{P}^{α} represents the orientation of the slip system α ; \mathbf{m}^{α} and \mathbf{n}^{α} are the slip direction vector and the slip plane normal vector of the slip system α , respectively. In the case of FCC materials, the number of active slip system N , is no more than the total slip system number, 12. The resolved shear stress τ^{α} acting on a particular slip system α , i.e., the *Schmid stress*, is given by the relation

$$\tau^{\alpha} = \boldsymbol{\sigma} : \mathbf{P}^{\alpha} \quad (5)$$

The shear rate of each slip system $\dot{\gamma}^{\alpha}$ can be related to the corresponding resolved shear stress τ^{α} via a power law expression,

$$\dot{\gamma}^{\alpha} = \left\langle \frac{|\tau^{\alpha} - x^{\alpha}| - Q^{\alpha}}{K} \right\rangle^n \text{sign}(\tau^{\alpha} - x^{\alpha}) \quad (6)$$

where x^{α} and Q^{α} are the kinematic and isotropic hardening variables of the slip system α , and are called as back resolved shear stress and isotropic deformation resistance, respectively. K and n are the material parameters that control the viscosity of the material.

The isotropic hardening rule involves an interaction matrix $H^{\alpha\beta}$ which represents the interaction between the systems α and β . The evolution rule of the isotropic hardening variable is determined by the following formulation,

$$\dot{Q}^{\alpha} = \sum_{\beta=1}^N H^{\alpha\beta} |\dot{\gamma}^{\beta}| \quad (7)$$

The initial value of Q^{α} means the initial shear yielding stress of each slip system, which is simply assumed as the same for all the slip systems in the model. The interaction hardening matrix $H^{\alpha\beta}$ is obtained from a simplified rule as shown in the work by Asaro (1983), i.e.,

$$H^{\alpha\beta} = qH + (1-q)H\delta_{\alpha\beta} \quad (8)$$

Whereas the nonlinear evolution rule of kinematic hardening is set to be similar to that proposed by Armstrong and Frederick (1966),

$$\dot{x}^{\alpha} = c\dot{\gamma}^{\alpha} - dx^{\alpha} |\dot{\gamma}^{\alpha}| \quad (9)$$

where c and d are the material parameters assumed to be the same for all slip systems. The fading memory term $dx^{\alpha} |\dot{\gamma}^{\alpha}|$ makes it possible to describe the ratchetting behavior of materials.

The proposed single crystal constitutive model is implemented numerically into the FE code ABAQUS via a user-defined material subroutine (UMAT), where the implicit integration is adopted.

Finite element model

Polycrystalline 5083 Al alloy may be viewed as an aggregation of single crystal grains with random crystallographic orientations, thus a 2D aggregation model is generated by using the Voronoi tessellation technique (Okabe et al. 1993), as shown in Fig. 1, where different colors indicate the grains with different orientations. To be consistent with corresponding experiments, the FE model is constructed as a rectangle plate with a size of 10 mm×6 mm. The FE mesh consists of 7040 first-order plane-stress elements.



Fig. 1. FE polycrystalline model (meshed)

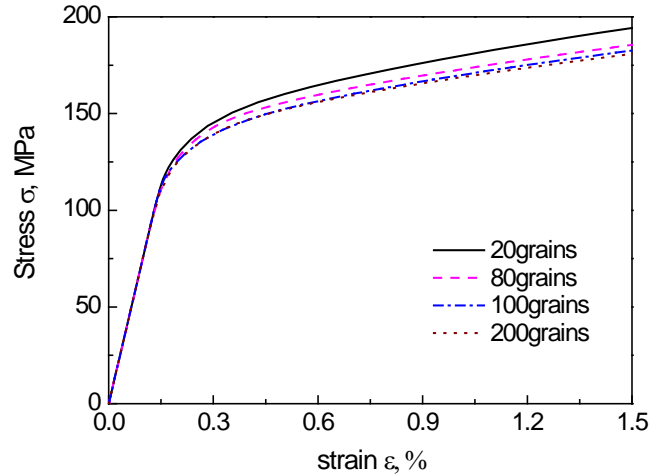


Fig. 2. Effect of number of grains on the stress-strain response

To eliminate the effect of random orientations as much as possible, sufficient number of grains is needed. A series of FE analyses containing 20, 80, 100, 200 grains are performed under monotonic tensile loading to assess the appropriate number of grains. It is seen in Fig. 2 that the further increase in the number of grains hardly influences the obtained stress-strain curves when the number of grains is larger than 100. Considering the computational efficiency, the following simulations are all based on the model containing 100 grains.

All material parameters used in the constitutive model for 5083 Al alloy are calibrated by trial-and-error method from the experimental results obtained under the monotonic tension, one of cyclic strain tests, and one of cyclic stress tests. The obtained material parameters are given in Table 1. Since there is no accurate anisotropic stiffness constant of 5083 Al alloy single crystal, and the main concern is focused on the macro responses of the polycrystalline alloy, the elastic parameters here are set to be isotropic. All the experimental results are carried out by Lu et al. (2013), and more details about experiments are referred to their work.

Table 1. Material parameters

Elasticity		Flow rule		Isotropic hardening	Interaction hardening	Kinematic hardening		
E (MPa)	ν	n	K (MPa)	Q_0 (MPa)	H (MPa)	q	c (MPa)	d
70,000	0.3	50	20	34	100	0	880	15

Simulation and discussion

To verify the validation of the model, the simulated results by the FE technique are compared with experimental ones of 5083 Al alloy plates obtained in the monotonic tension, uniaxial strain- and stress-controlled cyclic tests, respectively.

The simulated and experimental monotonic tensile stress-strain responses of polycrystalline 5083 Al alloy are shown in Fig. 3a at a strain rate of 0.015%/s. Clearly, the model simulation agrees quite well with the test data of monotonic tension. Fig. 3b shows the distribution of stress in the tensile direction when the macro monotonic tensile strain is 5%. Due to the different orientations of grains, the deformation is heterogeneous at both the inter-granular and intra-granular scales. From Fig. 3b it is seen that although the macroscopic state is in a tensile stress state, the heterogeneity still leads to a local microscopic compressive stress state. The load direction is denoted in Fig. 3b by a small arrow in the lower corner of right sideline.

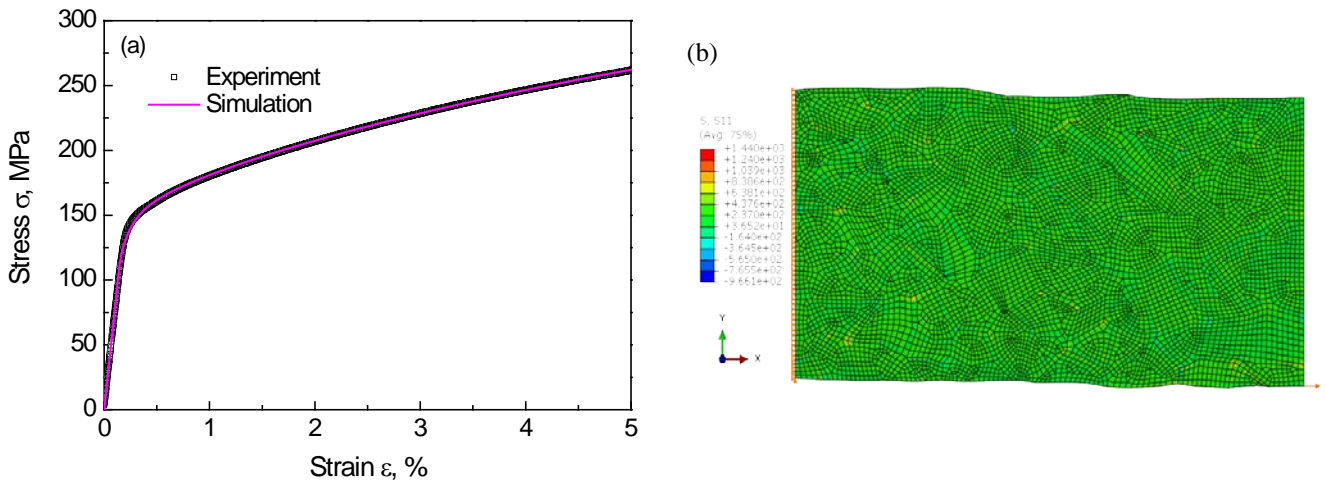


Fig. 3. Monotonic tensile responses: (a) comparison of simulated and experimental stress-strain curves; (b) simulated stress contour in the tensile direction.

The cyclic hardening behavior of 5083 Al alloy under uniaxial strain-controlled cyclic loading is then simulated and presented in Fig. 4 by plotting the stress-strain curves and variation of stress amplitude with the number of cycles. The strain rates in the load cases shown in Fig. 4 are fixed at 0.15%/s, the same as that used in the corresponding experiments.

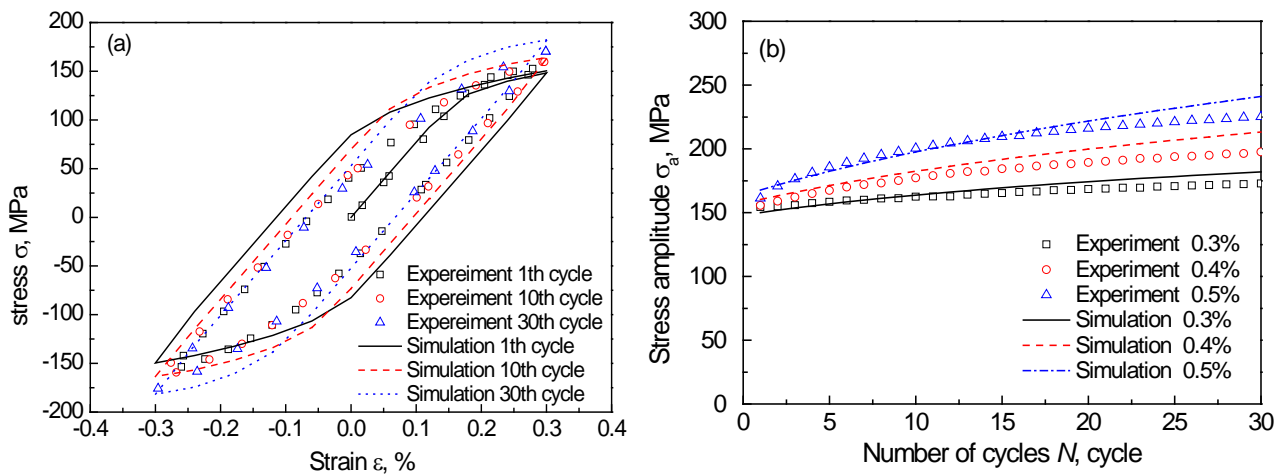


Fig. 4. Simulated and experimental responses under the strain-controlled cyclic loading: (a) cyclic stress-strain curves with a strain amplitude of 0.3%; (b) responded stress amplitude vs. number of cycles with different strain amplitudes.

Form Fig. 4a it can be found that the simulated hysteresis loops are a little wider than the experimental ones. This is caused by the delayed response of test machine and the practical peak strain cannot reach the prescribed value, especially in the first cycle. Fig. 4b shows the evolution curves of responded stress amplitude vs. number of cycles with three various applied strain

amplitudes. It is seen from Fig. 4b that the model provides a reasonable simulation to the cyclic hardening feature of the alloy, that is, the responded stress amplitude increases with the number of cycles, and the value of responded stress amplitude increases with the applied strain amplitude.

Finally, the ratchetting of 5083 Al alloy plates under the uniaxial stress-controlled cyclic loading with non-zero mean stress is predicted in the load cases with various mean stresses and stress amplitudes and compared with corresponding experiments. The results are shown in Fig. 5, and the stress rates in all the load cases are fixed at 80MPa/s, same as that used in the corresponding experiments. The comparison between simulated and experimental stress-strain hysteresis loops in the load case with a mean stress of 20MPa and stress amplitude of 160MPa is shown in Fig. 5a. It is seen from Fig. 5a that although the simulated loops are fatter than the experimental ones, the evolutionary process, that is the loops become narrower and narrower with the increasing number of cycles, is well simulated. The ratchetting strain obtained with various mean stresses and stress amplitudes are shown in Fig. 5b. It should be noted that the ratchetting strain ε_r is defined as $\varepsilon_r = (\varepsilon_{\max} + \varepsilon_{\min})/2$, where ε_{\max} and ε_{\min} are the maximum and minimum strains of each cycle, respectively. From Fig. 5b, it is concluded that the model can provide a reasonable simulation to the evolution of the uniaxial ratchetting and its dependence on the applied mean stress and stress amplitude. Or, specifically, the features include: (1) the ratchetting strain increases with the number of cycles, while its rate decreases as the number of cycles increases; (2) the ratchetting strain increases with the mean stress when the stress amplitude is fixed, and it also increases as the stress amplitude increases with a fixed mean stress; (3) after a certain number of cycles, the value of ratchetting strain hardly changes and the evolution of ratchetting falls into a stable state.

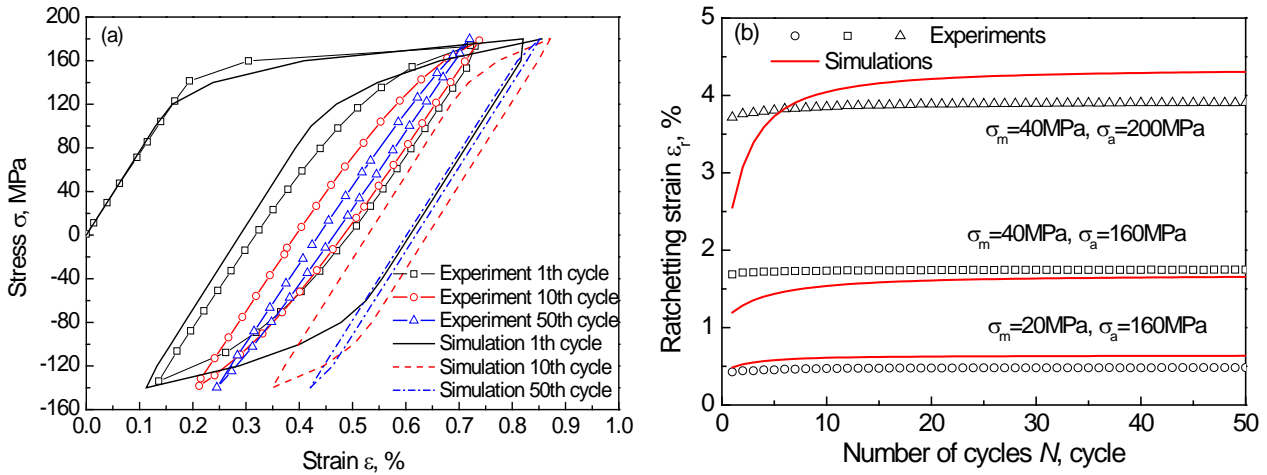


Fig. 5. Simulated and experimental ratchetting under cyclic stressing: (a) cyclic stress-strain curves; (b) curves of ratchetting strain vs. number of cycles.

Conclusion

In this paper, a crystal plasticity based cyclic visco-plastic constitutive model is implemented numerically into the finite element code, to predict the mechanical responses of polycrystalline metals under cyclic loading. A two-dimensional finite element aggregation consisting of 100 randomly orientated grains constructed by the Voronoi tessellation method is used to represent the polycrystalline metal. By comparing the FE simulated results with corresponding experimental ones, it is demonstrated that the model provides fairly good simulations to the macroscopic stress-strain responses of 5083 Al alloy plates under monotonic tension, the cyclic hardening feature presented under the strain-controlled cyclic loading, and the ratchetting occurred under the stress-controlled cyclic loading. Additionally, a local heterogeneous deformation is observed due to the orientation mismatch between the neighboring grains.

Acknowledgement

Financially supported by the projects for National Natural Science Foundation of China (11025210), Sichuan Provincial Youth Science and Technology Innovation Team (2013), China, and the project from National Key Laboratory of Traction Power (2011TPL-Z03).

References

- Abdel-Karim, M., Ohno, N. (2000), Kinematic hardening model suitable for ratcheting with steady-state. *Int. J. Plast.*, 16, pp. 225-240.
- Armstrong, P. J., Frederick, C. O. (1966), A mathematical representation of the multiaxial Bauschinger effect. CEGB Report RD/B/N 731. Berkeley Nuclear Laboratories, Berkeley, UK.
- Asaro, R. J. (1983), Crystal plasticity. *ASME J. Appl. Mech.* 50, pp. 921-934.
- Cailletaud, G., Sai, K. (2008), A polycrystalline model for the description of ratchetting: Effect of intergranular and intragranular hardening. *Mater. Sci. Eng. A*, 480(1-2), pp. 24-39.
- Chaboche, J. L., Dang Van, K., Cordier, G. (1979), Modelization of the strain memory effect on the cyclic hardening of 316 stainless steel. SMiRT'5, Div. L, Berlin, L11/3.
- Chaboche, J. L., Nouailhas, D. (1989), Constitutive modeling of ratcheting effect: Part II, Possibilities of some additional kinematic rules. *ASME J. Eng. Mater. Technol.* 111, pp. 384-416.
- Huang, Y. G. (1991), A user-material subroutine incorporating single crystal plasticity in the ABAQUS finite element program. Harvard University Report, MECH 178.
- Kang, G. Z., Bruhns, O. T., Sai, K. (2011), Cyclic polycrystalline visco-plastic model for ratchetting of 316L stainless steel. *Comput. Mater. Sci.* 50(4), pp. 1399-1405.
- Lu, F. C., Kang, G. Z., Liu, Y. J., Shi, K. K. (2013) Experimental study on uniaxial cyclic deformation of rolled 5083Al alloy plate. 7th ICLCF, Aachen, Germany.
- Okabe, A., Boots, B., Sugihara, K. (1993), Spatial tessellations: concepts and applications of Voronoi diagrams. *Computers & Geosciences*, 19 (8), pp. 1209-1210.
- Peirce, D., Asaro, R. J., Needleman, A. (1983), Material rate dependence and localized deformation in crystalline solids. *Acta Metall*, 31, pp. 1951-1976.